

Generalized Steppingstone Sampling: Efficient marginal likelihood estimation in gravitational wave analysis of Pulsar Timing Array data

El Mehdi Zahraoui,^{1*} Patricio Maturana-Russel,^{1,3} Willem van Straten,² Renate Meyer³ and Sergei Gulyaev¹

¹Department of Mathematical Sciences, Auckland University of Technology, Private Bag 92006, Auckland 1142, New Zealand

²Manly Astrophysics, 15/41-42 East Esplanade, Manly, NSW 2095, Australia

³Department of Statistics, University of Auckland, Auckland 1142, New Zealand

Accepted XXX. Received YYY; in original form ZZZ

ABSTRACT

Globally, Pulsar Timing Array (PTA) experiments have revealed evidence supporting an existing gravitational wave background (GWB) signal in the PTA data set. Apart from acquiring more observations, the sensitivity of PTA experiments can be increased by improving the accuracy of the noise modeling. In PTA data analysis, noise modeling is conducted primarily using Bayesian statistics, relying on the marginal likelihood and Bayes factor to assess evidence. We introduce generalized steppingstone (GSS) as an efficient and accurate marginal likelihood estimation method for the PTA-Bayesian framework. This method enables cheaper estimates with high accuracy, especially when comparing expensive models such as the Hellings-Downs (HD) model or the overlap reduction function model (ORF). We demonstrate the efficiency and the accuracy of GSS for model selection and evidence calculation by reevaluating the evidence of previous analyses from the North American Nanohertz Observatory for Gravitational Waves (NANOGrav) 15 yr data set and the European PTA (EPTA) second data release. We find similar evidence for the GWB compared to the one reported by the NANOGrav 15-year data set. Compared to the evidence reported for the EPTA second data release, we find a substantial increase in evidence supporting GWB across all data sets.

Key words: pulsar – gravitational waves – methods: statistical – methods: data analysis

1 INTRODUCTION

The pulsar timing array (PTA) emerged from the concept of a single pulsar-Earth baseline to observe gravitational waves (GW) in the low-frequency nanohertz band (Sazhin 1978). The PTA experiments were designed as a network of pulsars that could unveil the influence of GWs on the pulsating radio beams emitted from pulsars in the form of quadrupolar correlations (Hellings & Downs 1983). Millisecond pulsars (MSPs) became the key to achieving this objective due to their long-term stability, rivaling Earth's atomic clocks (Matsakis et al. 1997). Since the initial MSP timing analysis (Stinebring et al. 1990), the red noise (RN) in the MSPs' dataset has pointed to a promising future as observational radio astronomy and computational capability constantly improve. The next step for the PTA community was focused on gathering more data and refining the pulsar timing model to test and derive a realistic sensitivity threshold to observe GWs (Verbiest et al. 2009; Cordes & Shannon 2010; Hazboun et al. 2019). Recently, major PTA collaborations such as the North American Nanohertz Observatory for Gravitational Waves (NANOGrav; McLaughlin 2013), the Australian Parkes PTA (PPTA; Manchester et al. 2013), the European PTA (EPTA; Ferdman et al. 2010), the Indian PTA (InPTA; Joshi et al. 2018), reported positive statistical support for gravitational wave background (GWB) in the latest data

releases (Reardon et al. 2023; Agazie et al. 2023; Antoniadis et al. 2023b).

The PTA community has established a rigorous PTA-Bayesian framework (Van Haasteren et al. 2009), consistently expanding and acquiring new numerical and statistical techniques (Lentati et al. 2014; Johnson et al. 2024). This framework has enabled a simultaneous fit for different noise models and GWB signals while having the ability to compare the evidence of each different model (van Haasteren & Vallisneri 2014). Before evaluating the GWB evidence, it was proven that a common red signal (CRS) is evident across different PTA datasets: NANOGrav (Arzoumanian et al. 2020), EPTA (Chen et al. 2021), and PPTA (Goncharov et al. 2022). These findings resulted in a surge of interest in defining the nature of these CRSs and potentially revealing the buried GWB signal. Through this process, an extensive number of models were used to mitigate different sources of red noise that can affect the PTA's sensitivity either from pulsar contribution such as pulsar spin noise (Verbiest et al. 2009) and dispersion measure (DM) variations (Jones et al. 2017), or other noise sources such as spatial correlations due to the solar system ephemeris and the atomic clocks used in this experiment (Tiburzi et al. 2016). To test and account for all noise models, the full PTA-Bayesian analysis results in a large model space. Down the line, incorporating new MSP datasets and updated noise models will further expand this space significantly.

In the Bayesian framework, hypotheses comparison is done by evaluating the *Bayes factor*, which is the ratio of *marginal likelihoods*

* E-mail: elmehdi.zahraoui@autuni.ac.nz

of different models. This criterion is interpreted to assess the evidence for each hypothesis (Newton & Raftery 1994). For the PTA, model selection and evidence estimation are currently carried through various Bayesian techniques (Agazie et al. 2023; Antoniadis et al. 2023b). Among these methods, thermodynamic integration (TI; Lartillot & Philippe 2006) stands out as the cornerstone method for marginal likelihood estimation. In parallel, nested sampling (Skilling 2006) is implemented to provide not only estimates of marginal likelihood but also to generate posterior samples. Additionally, reweighting (Hourihane et al. 2023) was defined to estimate the marginal likelihood for an expensive model using an approximately matching model. Finally, the Hypermodel method, implemented using the Savage-Dickey density ratio approximation as a form of product space sampling for nested models (Carlin & Chib 1995; Lodewyckx et al. 2011), is routinely used across the whole PTA analyses. Johnson et al. (2024) discuss these methods in the context of the PTA, where nested sampling is used for models with small parameter spaces. In this case, nested sampling yields less accurate estimates with a similar cost to the Hypermodel method. In parallel, TI estimates become expensive for large PTA models and can lead to biased estimates if the required computational power is lacking. Consequently, TI is employed only where the Hypermodel fails to provide evidence estimates. Although the Hypermodel method was established as the predominant method, it is limited to nested models and requires assigning arbitrary weights to each model to avoid the Markov chain getting trapped in a particular model. Alternatively, we introduce generalized steppingstone sampling (GSS; Fan et al. 2011) as a new method to GW astronomy and in particular the PTA-Bayesian framework. GSS is intended to bypass most of the current issues with marginal likelihood estimation and provide an accurate marginal likelihood estimate at a cheaper computational price.

This article is structured as follows. Section 2 outlines model selection through the Bayes factor and briefly defines the TI, SS, and GSS methods. Section 3 demonstrates a comparison between these methods' performance applied to a Gaussian model. Thereafter, section 4 first discusses the implementation of GSS within the PTA framework. Then, our application to different PTA analyses will revisit the GWB evidence and will demonstrate the benefits of marginal likelihood estimation in making a robust model selection and monitoring the evidence on different CRS models. Finally, section 5 will discuss the prospects of GSS in the PTA-Bayesian framework and the significance of different PTA application results.

2 MARGINAL LIKELIHOOD ESTIMATION

The Bayesian framework is based on *Bayes'* theorem, which is given by

$$p(\theta|X, M) = \frac{L(X|\theta, M)\pi(\theta|M)}{z(X|M)} \quad (1)$$

for a model M and dataset X , where $\theta \in \Theta$ is the parameter vector, $p(\theta|X, M)$ the posterior probability density of θ , $L(X|\theta, M)$ the likelihood function and $\pi(\theta|M)$ the prior density. The constant $z(X|M)$, commonly denoted as z , is the *marginal likelihood*. The marginal likelihood is a multi-dimensional integral over the parameter space Θ defined by

$$z = \int_{\Theta} L(X|\theta, M)\pi(\theta|M)d\theta, \quad (2)$$

where $\pi(\theta|M)$ is a proper prior, i.e., $\int_{\Theta} \pi(\theta|M)d\theta = 1$. The integral z is a prior weighted average of the likelihood which quantifies the

goodness of fit of model M to data X . For a set of two models M_1 and M_2 fitted to a dataset X , the marginal likelihoods $z(X|M_1)$ and $z(X|M_2)$ can be used to compare these models such that the model with the higher marginal likelihood is preferred. Hence, the *Bayes factor* (BF), defined by

$$\text{BF}_{(M_1/M_2)} = \frac{z(X|M_1)}{z(X|M_2)}, \quad (3)$$

is used as a Bayesian criterion to compare M_1 to M_2 and perform model selection. Specifically, the *Bayes factor* is equivalent to the ratio of the posterior distributions of the models when the prior probabilities for the models are equal. In contrast, alternative performance tests are used to compare models such as the Bayesian information criterion (BIC) and the Akaike information criterion (AIC). Although the BIC and the AIC penalize unnecessary complexity by applying a uniform penalty for each parameter, these approaches ignore the importance of priors in the Bayesian analysis. The Bayes factor allows for tailored penalties based on the chosen priors which helps to ensure that overly complex models are penalized appropriately, reducing the risk of overfitting.

Apart from simple conjugate cases, the marginal likelihood has no analytical solution. In practice, considerable efforts have been made to numerically approximate z through Markov chain Monte Carlo (MCMC) methods such as the harmonic mean (Newton & Raftery 1994), bridge sampling (Meng & Wong 1996), and nested sampling (Skilling 2006). Path sampling (Gelman & Meng 1998) or thermodynamic integration (Lartillot & Philippe 2006) was the cornerstone technique of what would be later known as the method of power posterior (Friel & Pettitt 2008). This method defines a geometrical path that connects the prior with the posterior through the power posterior densities

$$p_{\beta}(\theta|X, M) = \frac{L(X|\theta, M)^{\beta}\pi(\theta|M)}{z_{\beta}} \quad \text{with } 0 \leq \beta \leq 1, \quad (4)$$

where β is the inverse temperature for the power posterior density p_{β} . When $\beta = 0$, the density p_{β} is equal to the prior distribution with $z_0 = 1$. When $\beta = 1$, the density p_{β} is equal to the posterior distribution resulting in $z_1 = z$. Correspondingly, thermodynamic integration relies on the identity

$$\log(z) = \int_0^1 E_{p_{\beta}}[\log(L(X|\theta, M))]d\beta, \quad (5)$$

where $E_{p_{\beta}}$ denotes the expected value with respect to p_{β} . For a sequence of β values, samples from each power posterior can be used to estimate the expected values by the sample averages. Thus, the integral in Equation (5) can be approximated using any technique for numerical integration, e.g., the trapezoidal rule. Thermodynamic integration can yield a good marginal likelihood estimate; nevertheless, it requires a high computational expense to produce a single estimate. This computational expense obliged modifications to the method to reduce the estimation cost. Steppingstone sampling was proposed as an attempt to reduce TI's cost, which resulted in a later far more efficient and accurate GSS method, which is considered one of the most accurate marginal likelihood estimation methods.

2.1 Steppingstone Sampling

The approximation of a continuous integral induces a discretization bias in TI leading to an inaccurate estimate of the marginal likelihood. Hence, steppingstone sampling was first proposed in the phylogenetics field (Xie et al. 2011) and later introduced to LIGO GW analysis (Maturana-Russel et al. 2019) as an alternative method

to enable unbiased estimates and improve model selection. The SS method estimates z through a product of sufficient $K-1$ intermediate ratios given by

$$z = \frac{z_1}{z_0} = \frac{z_{\beta_1}}{z_{\beta_0}} \frac{z_{\beta_2}}{z_{\beta_1}} \dots \frac{z_{\beta_{K-1}}}{z_{\beta_{K-2}}} = \prod_{k=1}^{K-1} \frac{z_{\beta_k}}{z_{\beta_{k-1}}}, \quad (6)$$

where $\beta_0 = 0 < \dots < \beta_{k-1} < \beta_k < \dots < \beta_{K-1} = 1$. Importance sampling can be used to estimate each of the ratios $r_k = z_{\beta_k}/z_{\beta_{k-1}}$, where $p_{\beta_{k-1}}$ acts as an excellent importance sampling distribution since $p_{\beta_{k-1}}$ is nearly identical to p_{β_k} for large K values. In this case, the ratio r_k can be written as

$$r_k = \int_{\Theta} \frac{L(X|\theta, M)^{\beta_k}}{L(X|\theta, M)^{\beta_{k-1}}} p_{\beta_{k-1}}(\theta|X, M) d\theta. \quad (7)$$

In practice, the r_k ratios are estimated using unbiased Monte Carlo estimator, therefore the MC estimate of the marginal likelihood is calculated by

$$\hat{z} = \prod_{k=1}^{K-1} \hat{r}_k = \prod_{k=1}^{K-1} \frac{1}{n} \sum_{i=1}^n L(X|\theta_{k-1,i}, M)^{\beta_k - \beta_{k-1}}, \quad (8)$$

with $\theta_{k-1,i}$ samples drawn from $p_{\beta_{k-1}}$ and n the number of drawn samples. To avoid numerical errors, it is preferable to work with $\log \hat{z}$. However, this transformation introduces a bias to the \hat{z} estimate which can be overcome by increasing K , the number of β chains (Xie et al. 2011). The choice of the β values and their dispersion can enhance the efficiency of SS and even more TI (Maturana-Russel et al. 2019; Xie et al. 2011). For β uniformly distributed along the quantiles of Beta($\alpha, 1$) distribution, it has been shown that the efficiency can be increased with $\alpha = 0.3$ for both methods (Xie et al. 2011).

2.2 Generalized Steppingstone Sampling

The performance of the steppingstone sampling reinforced the interest in decreasing the cost of marginal likelihood estimation while maintaining high accuracy. The generalized SS was proposed by Fan et al. (2011) to achieve this objective. The GSS method requires a distribution, referred to as the reference distribution π_0 , to shorten the path between the prior and the posterior. In practice, The reference distribution can be defined as the product of convenient distributions calibrated by posterior samples. The GSS defines a normalized density $f_{\beta} = q_{\beta}/c_{\beta}$ with the normalizing constant $c_{\beta} = \int_{\Theta} q_{\beta} d\theta$. By using the previous posterior definition, q_{β} is given by

$$q_{\beta} = [L(X|\theta, M)\pi(\theta|M)]^{\beta} [\pi_0(\theta|M)]^{1-\beta}. \quad (9)$$

For $\beta = 1$, f_{β} is equal to the posterior and $c_{\beta} = z$. In contrast to SS, if $\beta = 0$, f_{β} will be equal to the reference distribution π_0 and $c_{\beta} = 1$. For the GSS method, the ratio r_k becomes $c_{\beta_k}/c_{\beta_{k-1}}$, where $f_{\beta_{k-1}}$ is used as the importance sampling density. Fan et al. (2011) showed that when π_0 is introduced the mathematical expression of r_k becomes

$$r_k = E_{f_{\beta_{k-1}}} \left[\left(\frac{L(X|\theta, M)\pi(\theta|M)}{\pi_0(\theta|M)} \right)^{\beta_k - \beta_{k-1}} \right]. \quad (10)$$

The MC estimator of the ratio r_k rules out the largest sample η_k for numerical stability, and the log-MC estimator is given by

$$\log \hat{r}_k = (\beta_k - \beta_{k-1}) \log \eta_k + \log \left(\frac{1}{n} \sum_{i=1}^n \left[\frac{L(X|\theta_{k-1,i}, M)\pi(\theta_{k-1,i}|M)}{\eta_k \pi_0(\theta_{k-1,i}|M)} \right]^{\beta_k - \beta_{k-1}} \right), \quad (11)$$

with n samples $\theta_{k-1,i}$ from $f_{\beta_{k-1}}$ with

$$\eta_k = \max_{1 \leq i \leq n} \left[\frac{L(X|\theta_{k-1,i}, M)\pi(\theta_{k-1,i}|M)}{\pi_0(\theta_{k-1,i}|M)} \right]. \quad (12)$$

Finally, the log-marginal likelihood is estimated by summing over the ratios where

$$\log \hat{z} = \sum_{k=1}^{K-1} \log \hat{r}_k. \quad (13)$$

GSS inherits the benefits of the SS method and can be equal to SS if $\pi_0(\theta|M) = \pi(\theta|M)$. For GSS to be efficient, one can tailor a prior reference distribution π_0 that approximates the posterior as the product of independent distributions that reflect the distribution of each parameter θ . In practice, one is interested first in the parameter inference of the model M_1 so the posterior approximation is done before proceeding with model comparison. The posterior samples available from the approximation can be used to calibrate each probability density distribution of θ_j , where each distribution can be set for example to $\mathcal{N}(\mu_{\theta_j}, \sigma_{\theta_j}^2)$ with the mean and standard deviation of these samples. Similarly, it can be shown that for a target model T and an approximate model A with equal parameter space, the Reweighting method (Hourihane et al. 2023) is a particular case of the GSS method. In this case, the reference distribution π_0 is equal to $\text{likelihood} \times \text{prior}$ of the approximate model A with $K = 2$. The Reweighting method is particularly useful when the sampling from model T is computationally expensive.

3 SIMULATION STUDY

In this simulation study, we will implement the GSS method and compare its performance to that of SS and TI. Since the marginal likelihood z of real cases generally does not have an analytical solution, we resort to a simple Gaussian model where the marginal likelihood is known (Lartillot & Philippe 2006). This Gaussian model is parameterized by the vector $\theta = (\theta_1, \theta_2, \dots, \theta_d)$, where the prior on θ is a product of standard normal distributions $\theta_j \sim \mathcal{N}(0, 1)$, and the likelihood is defined by

$$L(\theta) = \prod_{j=1}^d \exp \left(-\frac{\theta_j^2}{2\nu} \right), \quad (14)$$

with d the number of dimensions, and ν the variance. This setup enables access to the analytical form for each component of the Bayesian model. The power posterior density can be expressed as a product of d normal distribution $\mathcal{N}(0, \nu/(v + \beta))$. The density p_{β} is equal to the posterior distribution when $\beta = 1$ yielding a marginal likelihood equal to

$$z = \left(\frac{\nu}{1 + \nu} \right)^{d/2}. \quad (15)$$

Since the analytical power posteriors are available, we sample directly from these densities to avoid MCMC sampling. For SS and TI, n independent samples are generated for each β_k chain, and then K the number of chains is increased until the numerical estimate reaches the true value. In contrast, the GSS estimator is executed in two steps. First, the independent samples from the posterior distribution (calibration samples N_{cal}) are used to configure the reference distribution, then n samples are generated for each β_k from the power

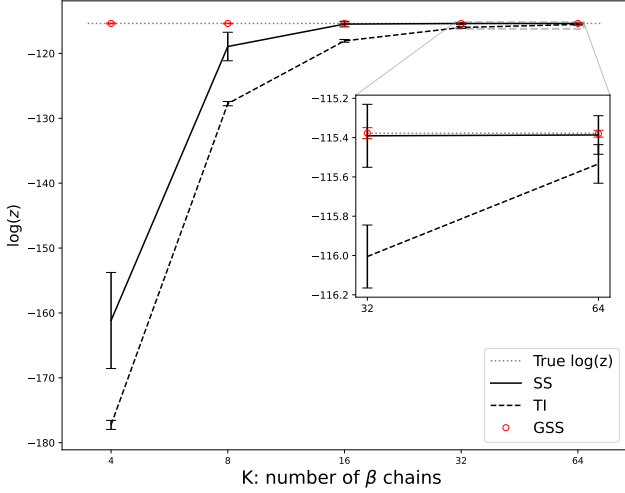


Figure 1. Comparison of log-marginal likelihood estimated as a function of K number of β chains for the Gaussian model with TI, SS, and GSS methods.

density $\mathcal{N}_{\beta_k,j}(\mu_{\beta_k,j}, \sigma_{\beta_k,j}^2)$ with

$$\mu_{\beta_k,j} = \frac{\bar{\theta}_j(1-\beta_k)}{S_j^2 \beta_k \left(\frac{1+\nu}{\nu}\right) + (1-\beta_k)}, \text{ and} \quad (16)$$

$$\sigma_{\beta_k,j}^2 = \left(\beta_k \left(\frac{1+\nu}{\nu}\right) + \frac{(1-\beta_k)}{S_j^2} \right)^{-1},$$

where $\bar{\theta}_j$ and S_j^2 are respectively the mean and the variance of the calibration samples from the j^{th} dimension.

For this comparison, we set the number of dimensions to $d = 50$ and variance to $\nu = 0.01$, resulting in a $\log(z) = -115.38$. With β_k uniformly dispersed along the quantiles of $\text{Beta}(0.3, 1)$, we fix $n = 1000$ independent sample, $K \in [4, 8, 16, 32, 64]$ number of β chains for each method. For the GSS estimator, the same setup is used, however, we set $N_{\text{cal}} = 1000$ and $n = 10$. To evaluate the uncertainty of each method's estimate, 1000 independent estimates are generated for each K . Figure 1 shows that TI requires more than 32 chains and 16 chains for SS to converge to the true $\log(z)$, while the GSS estimator yields an accurate estimate of $\log(\hat{z}) = -115.37$ with $K = 4$. This comparison demonstrates how the $\log(z)$ estimated using SS and TI can be biased even when error constraints are available. Thus, only increasing K will ensure convergence and an accurate $\log(z)$ estimate.

The GSS estimator's performance remains consistent with a higher number of dimensions as shown in Figure 2 where the number of dimensions $d = 2000$ and $N_{\text{cal}} = 500$. Figure 2 shows that one can either use fewer samples and increase K or use few β chains and increase n the number of samples per chain. In practice, numerical experiments suggest that the computational cost should be allocated to the number of β chains since a higher number of K increases the similarity between the consecutive importance distributions (Maturana-Russel 2017).

4 APPLICATION OF GSS TO THE PTA

In this section, we will illustrate how the GSS integrates into the PTA-Bayesian framework, and demonstrate the different benefits of

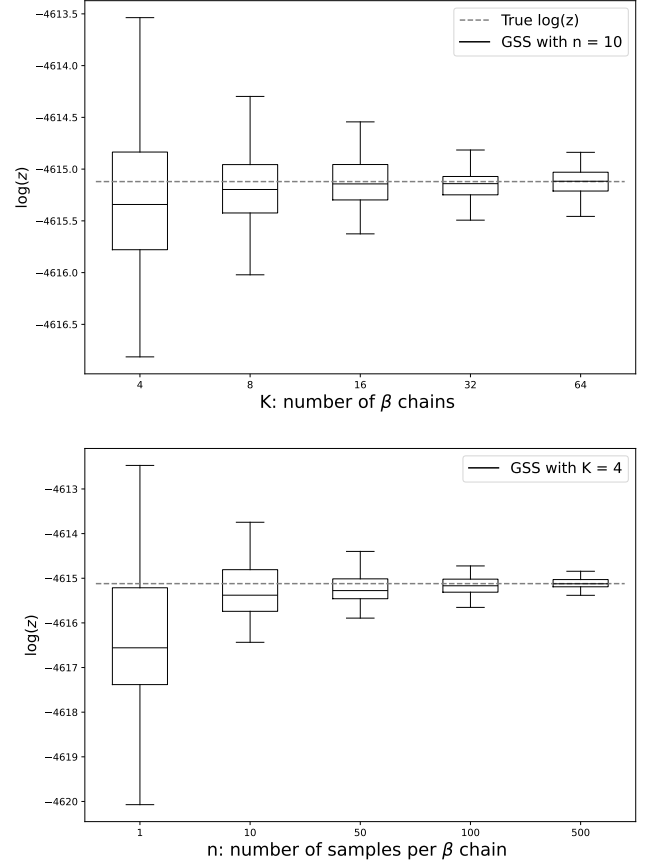


Figure 2. Convergence of the marginal likelihood estimated using GSS for the Gaussian model with $d = 2000$ and $\nu = 0.01$. Top panel: Comparison of log-marginal likelihood estimated as a function of K number of β chains with $n = 10$. Bottom panel: Comparison of log-marginal likelihood estimated as a function of n number of independent samples per β chains with $K = 4$.

estimating the *marginal likelihood* in a PTA analysis. For this application, a Metropolis-Hastings algorithm (Chib & Greenberg 1995) was implemented to perform the sampling for the GSS method, where MPI for Python (Dalcín et al. 2005) was employed to parallelize the sampling of β chains. This algorithm was designed to integrate into the common pipeline used in the PTA analyses (ENTERPRISE; Ellis et al. 2019; Taylor et al. 2021). In the following, the performance of GSS is assessed based on K , the number of β chains, and n_{ESS} the effective sample size (ESS) per β chain. We will use the GSS method to produce multiple independent estimates for each single analysis. These multiple estimates allow the direct comparison of all models by constructing a distribution of the Bayes factor of the compared models. In practice, single random draws of $\log(\hat{z})$ from the marginal likelihood distributions for model M_1 and M_2 are used to compute each $\log(\text{BF}_{M_1/M_2})$, the standard deviation of the resulting $\log(\text{BF}_{M_1/M_2})$ distribution is used to measure uncertainty.

4.1 Application to NANOGrav

This section demonstrates the application of the GSS to estimate the marginal likelihood for different models used in the PTA single pulsar noise analysis and GWB analysis. We reproduce the analysis and the public NANOGrav 15yr Data Release and the NANOGrav tutorials (Agazie et al. 2023) using ENTERPRISE pipeline. The consistency

of the reproduced Bayesian analysis is compared with the results discussed in the NANOGrav 15 yr Data Set.

4.1.1 Model selection for single pulsar analysis

The following four pulsars were selected from NANOGrav (Agazie et al. 2023) as candidates for single-pulsar noise analysis: PSRs J1012+5307, J1600-3053, J1705-1903, and J1713+0747. Around 100,000 posterior samples are generated for each combination of the following noise models: white noise (WN), dispersion measure Gaussian process (DMGP), and red noise (RN). A 20,000 sample of the burn-in period is discarded from the posterior samples of each parameter to calibrate the reference distribution π_0 . In this case, the posterior samples are reasonably unimodal and often symmetric, therefore, for each model a normal distribution is used to approximate each parameter's marginal posterior distribution. The product of these distributions defines the reference distribution π_0 , as it usually provides a sufficiently accurate approximation to the posterior for the GSS method. The mean and the variance of each parameter's set of samples are used to calibrate π_0 , then a mean effective sample size $n_{\text{ESS}} \approx 10$ is generated for each β chain with $K = 8$ for each single estimate. Table 1 reports the mean and standard deviation of 100 independent $\log(\hat{z})$ for the combination of the three noise models. These values of $\log(\hat{z})$ are used to compute the $\log(\widehat{\text{BF}})$ for comparing models' relative performance.

For each pulsar, the WN model is used as a baseline for model comparison, the best-performing model compared to WN is reported with their $\log(\widehat{\text{BF}}_{M/\text{WN}}) \pm 1\sigma$. Across all four pulsars, strong statistical evidence is observed for the Red Noise model. For PSR J1012+5307, WN+RN is favored with $\log(\widehat{\text{BF}}) = 36.47 \pm 0.56$. When combined with the other two models, the DMGP model has weak statistical evidence since $\log(\widehat{\text{BF}}) < 1$. For PSR J1705-1903 and PSR J1713+0747, the model comparison shows high statistical significance between each fitted model, where the most significant model is WN+RN+DMGP with $\log(\widehat{\text{BF}}) = 129.07 \pm 0.49$ for PSR J1705-1903, and WN+RN with $\log(\widehat{\text{BF}}) = 342.58 \pm 3.29$ for PSR J1713+0747. PSR J1600-3053 demonstrates the least RN significance compared to the other 3 pulsars with $\log(\widehat{\text{BF}}) = 5.56 \pm 0.99$. The evidence of the excess noise becomes more significant for the model WN+RN+DMGP with $\log(\widehat{\text{BF}}) = 6.00 \pm 1.05$.

One can further examine the performance of each model by inspecting the influence of its parameters δ when included. This influence can be demonstrated for the PTA models using the previous combinations of red noise models. This evaluation can be conducted using the *Inclusion Bayes factor* (IBF; Hinne et al. 2020) which examines the proportional change of the marginal likelihood when a set of parameters δ are included in a set of models. Let \mathcal{M}_{δ^1} and \mathcal{M}_{δ^0} be respectively the sets of models that include and exclude δ from their respective parameter vector. The IBF is given by

$$\text{IBF} = \frac{\sum_{M \in \mathcal{M}_{\delta^1}} z(X|M)}{\sum_{M \in \mathcal{M}_{\delta^0}} z(X|M)}, \quad (17)$$

which denotes the sum of marginal likelihoods of models including δ divided by the sum of marginal likelihoods of models excluding it. Table 2 shows the IBF to compare the overall performance of RN and DMGP parameters. IBF reinforces the strong statistical evidence of RN across all pulsars while including DMGP parameters delivers a better performance only for PSR J1705-1903 and PSR J1713+0747. Since pulsar customized noise models are used for the full GWB analysis, the IBF can provide additional statistical evidence and help with a robust model selection where decisions are critical.

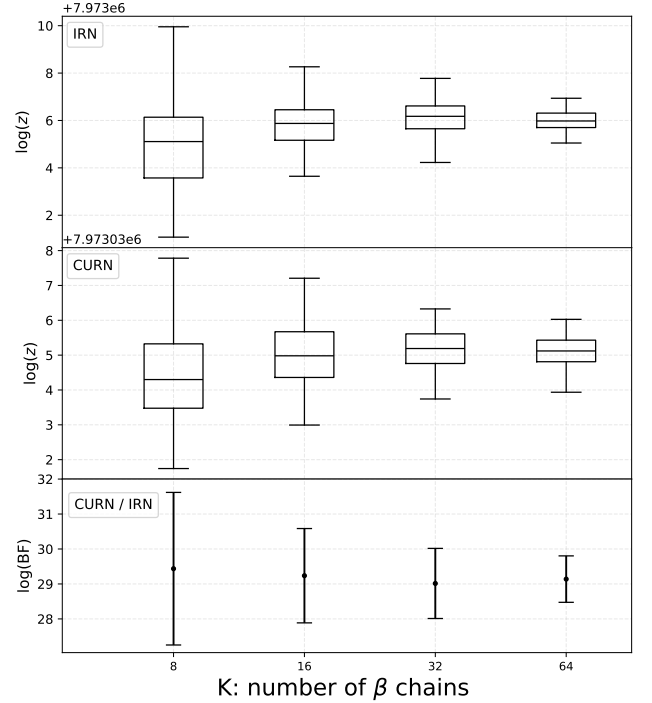


Figure 3. Estimations as a function of K number of β chains for the NANOGrav dataset via GSS. Top panel: \log -marginal likelihood estimated for the IRN model. Middle panel: \log -marginal likelihood estimated for the CURN model. Bottom panel: $\log(\widehat{\text{BF}}_{\text{CURN/IRN}})$ comparing CURN to IRN.

4.1.2 Evidence estimation for the GWB analysis

In parallel with our previous analysis, the GSS estimator can also be used to investigate the evidence of GWB in the PTA. We reproduce the posteriors used in the NANOGrav analysis where all CRS models share the log-spectral amplitude $\log(A_M)$ and the spectral index γ_M of the power law as free parameters for the four following models: intrinsic red noise (IRN), common uncorrelated red noise (CURN), spline overlap reduction function (Spl ORF), and the Hellings and Downs (HD) serving as the probe for GWB. The default setup and codes provided by the NANOGrav public data release are used in this demonstration. We refer to Agazie et al. (2023) for extended details on the setup and the models. In this case, around 120,000 samples are generated for each of the 4 models. Before estimating $\log(z)$, the posterior samples are compared with the previous analyses for consistency. The means and the standard deviations of the generated samples are in agreement with the reported results in Agazie et al. (2023).

To configure the GSS, a 20,000 sample of the burn-in period is discarded from the posterior samples used to calibrate the reference distribution π_0 . By tuning the reference distribution and using it as a sampling proposal distribution, the GSS estimator enables us to skip the new burn-in period in the GSS sampling. In Figure 3, each $\log(z)$ estimate is computed using $n_{\text{ESS}} \approx 50$ per each β chain, while the number of parallel chains grows with $K \in [8, 16, 32, 64]$. A higher number of n_{ESS} is used to cross-check the consistency of the $\log(\hat{z})$ estimates. As demonstrated in Figure 3, the GSS estimator produces a consistent median over 100 $\log(\hat{z})$ starting from $K = 16$ while constraining the uncertainty as the number of chains increases, a higher number of n_{ESS} can improve the estimate of the median $\log(\hat{z})$ for $K = 8$ as shown in Figure 2. The $\log(\widehat{\text{BF}})$ is consistent through all K and the slight variation would not affect the inference.

Table 1. Mean and standard deviation of 100 independent log-marginal likelihood estimates for NANOGrav single pulsar noise models obtained via GSS with $K = 8$.

PSR	WN		WN+DMGP		WN+RN		WN+RN+DMGP	
	$\log(\hat{z})$	std	$\log(\hat{z})$	std	$\log(\hat{z})$	std	$\log(\hat{z})$	std
J1012+5307	299450.92	0.20	299450.97	0.25	299487.46	0.48	299488.38	0.61
J1600-3053	282873.05	0.57	282873.11	0.65	282878.61	0.81	282879.06	0.87
J1705-1903	120575.24	0.29	120671.36	0.32	120633.48	0.44	120704.32	0.41
J1713+0747	805517.65	3.24	805521.53	1.18	805860.37	0.78	805859.78	2.13

PSR	DMGP		RN	
	$\log(\widehat{\text{IBF}})$	std	$\log(\widehat{\text{IBF}})$	std
J1012+5307	0.99	0.87	73.94	0.82
J1600-3053	0.52	1.41	11.42	1.43
J1705-1903	166.92	0.75	91.20	0.74
J1713+0747	3.46	4.14	680.88	4.17

Table 2. Mean and standard deviation of 1000 independent $\log(\widehat{\text{IBF}})$ estimates for the parameter inclusion of DMGP model and RN model in NANOGrav single pulsar noise models.

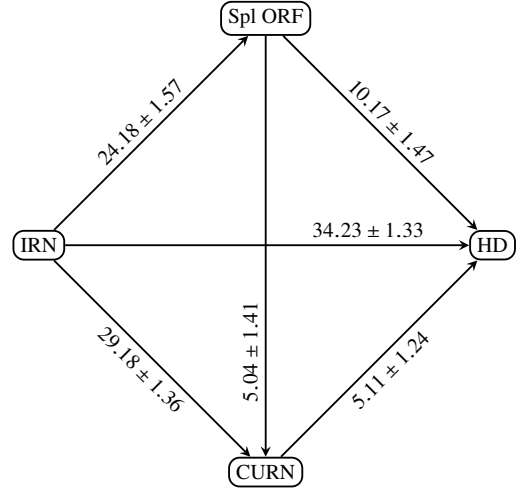
	$\log(\hat{z})$	std
IRN	7973005.73	1.07
CURN	7973034.93	0.84
Spl ORF	7973029.96	1.18
HD	7973040.01	0.91

Table 3. Mean and standard deviation of 100 independent log-marginal likelihood estimates with $K = 16$ for different common red process models in the NANOGrav dataset.

To evaluate the GWB evidence, 100 independent estimates were computed for each of the four models, Table 3 reports the mean and the standard deviation of 100 estimates of $\log(\hat{z})$. Figure 4 reports the mean and standard deviation where 1000 estimates of $\log(\widehat{\text{BF}})$ were derived to compare the models. Compared to IRN, the other three models are highly supported reinforcing the strong evidence of an extra red process in the PTA dataset. Furthermore with a $\log(\widehat{\text{BF}}_{\text{CURN/IRN}})$ of 29.18 ± 1.36 , a common uncorrelated red noise process is evident in the dataset reconfirming the previous PTA analyses (Arzoumanian et al. 2020; Chen et al. 2021; Goncharov et al. 2022). Currently, CURN is favored over the Spl ORF model with $\log(\widehat{\text{BF}}_{\text{CURN/Spl ORF}}) = 5.04 \pm 1.41$. For the GWB evidence, $\log(\widehat{\text{BF}}_{\text{HD/CURN}}) = 5.11 \pm 1.24$ is consistent with the NANOGrav reported estimation of 5.42 ± 4.25 , whereas the uncertainty is more constrained by the GSS method.

4.2 Application to EPTA+InPTA

The EPTA+InPTA collaboration has publicly released its second dataset with the analysis for GW evidence (Antoniadis et al. 2023b). This analysis combines the dataset of 25 pulsars into four subsets:

**Figure 4.** Mean and standard deviation of 1000 independent $\log(\widehat{\text{BF}}_{M_1/M_2})$ estimates comparing different common red process models in the NANOGrav dataset where the arrow starts at model M_2 and ends at model M_1 .

DR2full covers 24.7 years of EPTA data, DR2new is limited to the last 10.3 years of observations with the upgraded radio telescopes, DR2full+ and DR2new+ adds 0.7 years of InPTA data to the previous subsets. The EPTA+InPTA study uses customized pulsar noise models reported in Antoniadis et al. (2023a). We will reproduce the analysis using the 4 subsets for the following models CURN, GWB (referred to as HD in section 4.1.2), and Binned ORF by using the default setup provided in the second data release. Around 120,000 posterior samples are generated for each model, and then their means and standard deviations are examined for consistency with the reported ones in Antoniadis et al. (2023b). A burn-in period of the first 20,000 samples was discarded from the posterior samples used to calibrate the reference distribution π_0 . A 100 $\log(\hat{z})$ per model are estimated with $K = 16$ and $n_{\text{ESS}} \approx 20$ samples per β chain. To assess the stability of the estimation, n_{ESS} and K are increased and $\log(\hat{z})$ estimates are cross-checked for consistency.

Table 4 reports the mean and the standard deviation of 100 $\log(\hat{z})$ estimates for the 3 models across all EPTA+InPTA datasets. To compare each model's performance, Table 5 reports the mean and the standard deviation of 1000 $\log(\widehat{\text{BF}}_{M/\text{CURN}})$ independent estimates of the other two models compared to the CURN model. For DR2full and DR2full+, the $\log(\widehat{\text{BF}}_{\text{GWB/CURN}})$ supports the GWB model over the CURN model. This support is further reinforced when fitting only to the new generation dataset DR2new. However, CURN model is favored over the Binned ORF model, and this evidence decreases for DR2new. The addition of the InPTA dataset in DR2full+ and

Table 4. Mean and standard deviation of 100 log-marginal likelihood estimates for each common red process model applied to the EPTA+InPTA datasets with $K = 16$.

	DR2new		DR2new+		DR2full		DR2full+	
	$\log(\bar{z})$	std	$\log(\bar{z})$	std	$\log(\bar{z})$	std	$\log(\bar{z})$	std
PSRN+CURN	535429.85	1.02	572146.21	1.08	658725.61	1.20	695438.21	1.03
PSRN+Binned ORF	535427.40	1.30	572143.38	1.36	658721.80	1.31	695434.63	1.05
PSRN+GWB	535438.09	1.14	572154.12	0.98	658731.26	1.12	695444.04	1.01

Table 5. Mean and standard deviation of 1000 independent $\log(\widehat{\text{BF}}_{\text{M/CURN}})$ estimates comparing Binned ORF and GWB model to CURN model across EPTA+InPTA datasets.

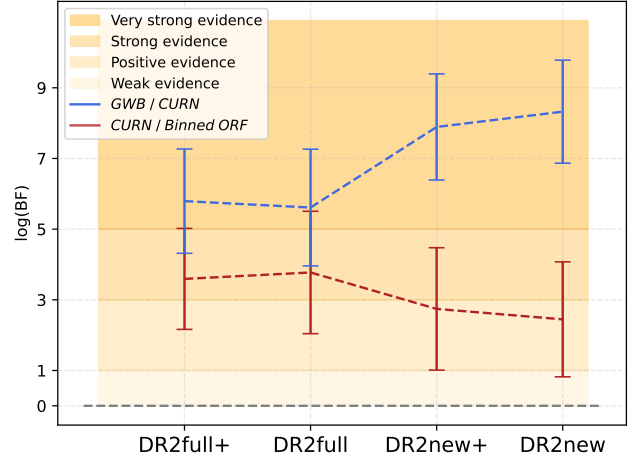
Model	DR2new		DR2new+		DR2full		DR2full+	
	$\log(\widehat{\text{BF}})$	std	$\log(\widehat{\text{BF}})$	std	$\log(\widehat{\text{BF}})$	std	$\log(\widehat{\text{BF}})$	std
PSRN+Binned ORF	-2.35	1.65	-2.81	1.76	-3.62	1.42	-3.80	1.81
PSRN+GWB	8.24	1.47	7.89	1.48	5.79	1.42	5.70	1.57

DR2new+ slightly decreases the evidence on the GWB model and slightly increases the evidence favoring CURN over Binned ORF. Figure 5 summarizes this evolution of evidence in the EPTA+InPTA dataset. Although the InPTA dataset is recent the slight decrease in evidence of GWB might arise from adding 1 year of dataset contributing asymmetrically to only 12 pulsars out of 25 candidates which will directly affect the correlations between pulsars.

5 DISCUSSION

In the simulation study, we highlighted the difference between methods of power posterior and showed their relative performance. The GSS method has outperformed both TI and SS and proved efficient for higher dimensional cases. GSS can benefit from the previous efforts usually done in the parameter estimation phase. The success of a cheaper GSS estimation relies on having a good posterior approximation which shortens the path to an accurate estimate. Without such an approximation, the GSS estimator will require more effort (but still less than SS and TI) to achieve an accurate estimate. These $\log(z)$ estimates result in an accurate evaluation of the $\log(\text{BF})$ and robust interpretation of evidence supporting different hypotheses. This evidence can further be tested using the IBF criteria, which examines the influence of a particular set of parameters on the evidence.

Due to its cheaper cost, the GSS method enabled multiple $\log(z)$ estimates with high accuracy for each PTA-Bayesian analysis in this study. For single noise analysis, GSS has shown its ability to offer model selection without constraints, compared to the Hypermodel that can fail to provide evidence evaluation in cases such as estimation for RN cases (Smarra et al. 2023). In the NANOGrav dataset, the four pulsars have shown different levels of significance for RN and DMGP signals, where PSR J1713+0747 showed extreme evidence for RN. Note that PSR J1713+0747 contributed the most to the common red noise signal in the EPTA+InPTA dataset (Antoniadis et al. 2023b). For NANOGrav GWB evidence, the GSS method has provided a consistent and more accurate estimate than the Hypermodel method of evidence supporting a GWB signal compared to a common red noise signal. Furthermore, GSS enabled a direct comparison of expensive models efficiently eliminating the arbitrary

**Figure 5.** Evolution of $\log(\widehat{\text{BF}}_{\text{M}_1/\text{M}_2})$ comparing different common red process models as a function of the dataset size of EPTA+InPTA dataset with DR2full+ the full dataset and DR2new the shortest subset.

weights required by the Hypermodel method. The EPTA GWB analysis consistently reconfirms the evidence supporting a GWB signal in the PTA dataset. This evidence becomes more significant for the new-generation dataset as shown in Figure 5.

The PTA experiments rely on model selection to tune each part of the Bayesian noise model which increases the number of Bayesian analyses required to achieve better sensitivity. The current GSS setup substantially minimized the cost of a single $\log(z)$ estimate for both light and expensive models, and would further benefit in the future from better samplers. The efficiency of the GSS method will help reduce the cost of evidence estimation for the continuously growing model portfolio for GWs and new physics in the PTA (Afzal et al. 2023; Smarra et al. 2023).

ACKNOWLEDGMENTS

PMR, WS, and RM gratefully acknowledge support by the Marsden Fund Council grant MFP-UOA2131 from New Zealand Government funding, managed by the Royal Society Te Apārangi. This work was performed on the OzSTAR national facility at Swinburne University of Technology. The OzSTAR program receives funding in part from the Astronomy National Collaborative Research Infrastructure Strategy (NCRIS) allocation provided by the Australian Government, and from the Victorian Higher Education State Investment Fund (VHE-SIF) provided by the Victorian Government.

Software: ENTERPRISE (Ellis et al. 2019; Taylor et al. 2021), `enterprise_extension` (Taylor et al. 2021), PTMCMC (Ellis & van Haasteren 2017), `MPI4PY` (Dalcín et al. 2005), `Jupyter` (Kluyver et al. 2016), `matplotlib` (Hunter 2007), `numpy` (Harris et al. 2020), `scipy` (Virtanen et al. 2020), `arviz` (Kumar et al. 2019).

DATA AVAILABILITY

Data used in this analysis are available on GSS-estimator GitHub¹.

REFERENCES

- Afzal A., et al., 2023, *The Astrophysical Journal Letters*, 951, L11
- Agazie G., et al., 2023, *The Astrophysical Journal Letters*, 951, L8
- Antoniadis J., et al., 2023a, *Astronomy & Astrophysics*, 678, A49
- Antoniadis J., et al., 2023b, *Astronomy & Astrophysics*, 678, A50
- Arzoumanian Z., et al., 2020, *The Astrophysical Journal Letters*, 905, L34
- Carlin B. P., Chib S., 1995, *Journal Of The Royal Statistical Society Series B: Statistical Methodology*, 57, 473
- Chen S., et al., 2021, *Monthly Notices of the Royal Astronomical Society*, 508, 4970
- Chib S., Greenberg E., 1995, *The American Statistician*, 49, 327
- Cordes J. M., Shannon R. M., 2010, A Measurement Model for Precision Pulsar Timing (arXiv:1010.3785), <https://arxiv.org/abs/1010.3785>
- Dalcín L., Paz R., Storti M., 2005, *Journal of Parallel and Distributed Computing*, 65, 1108
- Ellis J., van Haasteren R., 2017, `jellisl8/PTMCMCSampler: Official Release`, doi:10.5281/zenodo.1037579, <https://doi.org/10.5281/zenodo.1037579>
- Ellis J. A., Vallisneri M., Taylor S. R., Baker P. T., 2019, *Astrophysics Source Code Library*, pp ascl-1912
- Fan Y., Wu R., Chen M.-H., Kuo L., Lewis P. O., 2011, *Molecular biology and evolution*, 28, 523
- Ferdman R. D., et al., 2010, *Classical and Quantum Gravity*, 27, 084014
- Friel N., Pettitt A. N., 2008, *Journal of the Royal Statistical Society Series B: Statistical Methodology*, 70, 589
- Gelman A., Meng X.-L., 1998, *Statistical Science*, pp 163–185
- Goncharov B., et al., 2022, *The Astrophysical Journal Letters*, 932, L22
- Harris C. R., et al., 2020, *Nature*, 585, 357
- Hazboun J. S., Romano J. D., Smith T. L., 2019, *Physical Review D*, 100, 104028
- Hellings R., Downs G., 1983, *Astrophysical Journal, Part 2-Letters to the Editor*, vol. 265, Feb. 15, 1983, p. L39-L42., 265, L39
- Hinne M., Gronau Q. F., van den Bergh D., Wagenmakers E.-J., 2020, *Advances in Methods and Practices in Psychological Science*, 3, 200
- Hourihane S., Meyers P., Johnson A., Chatziioannou K., Vallisneri M., 2023, *Physical Review D*, 107, 084045
- Hunter J. D., 2007, *Computing in Science & Engineering*, 9, 90
- Johnson A. D., et al., 2024, *Phys. Rev. D*, 109, 103012
- Jones M. L., et al., 2017, *The Astrophysical Journal*, 841, 125
- Joshi B. C., et al., 2018, *Journal of Astrophysics and Astronomy*, 39, 51
- Kluyver T., et al., 2016, in , Positioning and power in academic publishing: Players, agents and agendas. IOS press, pp 87–90, doi:10.3233/978-1-61499-649-1-87
- Kumar R., Carroll C., Hartikainen A., Martin O., 2019, *Journal of Open Source Software*, 4, 1143
- Lartillot N., Philippe H., 2006, *Systematic Biology*, 55, 195
- Lentati L., Alexander P., Hobson M. P., Feroz F., van Haasteren R., Lee K., Shannon R. M., 2014, *Monthly Notices of the Royal Astronomical Society*, 437, 3004
- Lodewyckx T., Kim W., Lee M. D., Tuerlinckx F., Kuppens P., Wagenmakers E.-J., 2011, *Journal of Mathematical Psychology*, 55, 331
- Manchester R., et al., 2013, *Publications of the Astronomical Society of Australia*, 30, e017
- Matsakis D. N., Taylor J. H., Eubanks T. M., 1997, *Astronomy and Astrophysics*, v. 326, p. 924-928, 326, 924
- Maturana-Russel P. A., 2017, PhD thesis, University of Auckland, <https://researchspace.auckland.ac.nz/docs/uaa-docs/rights.htm>
- Maturana-Russel P., Meyer R., Veitch J., Christensen N., 2019, *Physical Review D*, 99, 084006
- McLaughlin M. A., 2013, *Classical and Quantum Gravity*, 30, 224008
- Meng X.-L., Wong W. H., 1996, *Statistica Sinica*, pp 831–860
- Newton M. A., Raftery A. E., 1994, *Journal of the Royal Statistical Society Series B: Statistical Methodology*, 56, 3
- Reardon D. J., et al., 2023, *The Astrophysical Journal Letters*, 951, L6
- Sazhin M. V., 1978, *Soviet Ast.*, 22, 36
- Skilling J., 2006, *Bayesian Analysis*, 1, 833
- Smarra C., et al., 2023, *Physical Review Letters*, 131, 171001
- Stinebring D., Ryba M., Taylor J. H., Romani d. R., 1990, *Physical Review Letters*, 65, 285
- Taylor S. R., Baker P. T., Hazboun J. S., Simon J., Vigeland S. J., 2021, `enterprise_extensions`, https://github.com/nanograv/enterprise_extensions
- Tiburzi C., et al., 2016, *Monthly Notices of The Royal Astronomical Society*, 455, 4339
- Van Haasteren R., Levin Y., McDonald P., Lu T., 2009, *Monthly Notices of the Royal Astronomical Society*, 395, 1005
- Verbiest J., et al., 2009, *Monthly Notices of the Royal Astronomical Society*, 400, 951
- Virtanen P., et al., 2020, `scipy/scipy: SciPy 1.6.0`, doi:10.5281/zenodo.4406806, <https://doi.org/10.5281/zenodo.4406806>
- Xie W., Lewis P. O., Fan Y., Kuo L., Chen M.-H., 2011, *Systematic Biology*, 60, 150
- van Haasteren R., Vallisneri M., 2014, *Physical Review D*, 90, 104012

This paper has been typeset from a $\text{\TeX}/\text{\LaTeX}$ file prepared by the author.

¹ <https://github.com/nz-gravity/GSS-estimator>